Energy Equip. Sys./ Vol. 10/No. 4/Dec. 2022/ 353-374

ENERGY EQUIPSYS

Energy Equipment and Systems

http://energyequipsys.ut.ac.ir
www.energyequipsys.com

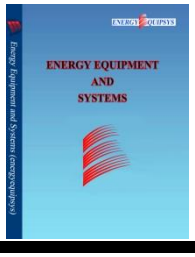

Numerical investigation on thermal performance enhancement of a flat-plate natural flow double-pass solar air heater – The effect of the absorber plate

Authors

Amir Babak Ansari [a*]
Seyyed Abdolreza Gandjalikhan Nassab [b]

[a] Department of Energy, Institute of Science and High Technology and Environmental Sciences, Graduate University of Advanced Technology, Kerman, Iran

[b] Mechanical Engineering Department, School of Engineering, Shahid Bahonar University of Kerman, Kerman, Iran

Article history:

Received : 16 September 2021
Accepted : 24 December 2021

ABSTRACT

The main contribution of this study is to highlight the position effect of the absorber plate as a passive heat transfer enhancement technique on the ventilation and thermal performance of a solar air heater, including outlet air temperature, airflow rate, and thermal efficiency. The turbulent free convection heat transfer in a vertical flat-plate solar air heater with single and double passes is numerically studied. A total of four cases of airflow (three double-pass and one single-pass air heater) are simulated and compared. The set of transient governing equations, including the continuity, momentum, and energy are solved to simulate the turbulent free convection airflow inside the heater based on the $\kappa-\varepsilon$ *turbulence model, while the transient conduction equation is solved inside the solid elements, i.e., bottom plat, absorber, and glass cover based on the finite-element method. The results reveal that the position of the absorber plate has a double-edged sword impact on the performance of solar air heaters, including the airflow rate and outlet air temperature. Moreover, a 100% increase in the natural air flow rate is observed for the double-pass heater compared to the single-pass one. Moreover, a 15% improvement in thermal efficiency can be obtained from 68% to 78% in the double-pass solar air heater based on the position of the absorber plate. Based on the criteria, including the outlet temperature, airflow rate, or thermal efficiency, the presented results can be used as a good reference to choose an alternative for solar air heaters.*

Keywords: Double-Pass Solar Air Heater; Natural Turbulent Convection; Space Heating; Heat Transfer Enhancement; Absorber Plate.

1.Introduction

Solar air heaters (SAH) have been substantially used in many applications with low to moderate temperature demands, which has been of great concern to researchers and engineers in recent years. According to their geometries and flow patterns, they are classified into different types, including single- or multiple-pass, parallel or counter-flow configuration, natural or forced convective flow, etc. Solar air heaters are cost-effective and easily installed, in which the solar radiation warms up the cold air, which may be

* corresponding author: Amir Babak Ansari
Department of Energy, Institute of Science and High Technology and Environmental Sciences, Graduate University of Advanced Technology, Kerman, Iran
Email: a.b.ansari@kgut.ac.ir

used for many engineering applications such as space heating [1,2], drying agricultural products [3,4], air condition systems [5,6], preheating for industrial applications [7], desalination systems [8], etc. Among widely mentioned applications, space heating is the main contribution of the present study. Choudhury and Baruah [9] presented a review on the importance of solar air heaters in space heating of residential applications in which some issues were of great concern, including installation constraints, output temperature, balancing between demand and supply, and so on. Moreover, to increase the reliability of SAHs, using modular design was also investigated as a performance improvement suggestion in residential space heating. Flat-plate solar air heaters with natural convection flow have been widely investigated for space heating purposes. Shi et al. [10] presented an empirical model of a solar chimney placed on the roof to enhance the ventilation inside a building. The effect of geometrical parameters, including inclination angle, inlet and outlet section areas, air gap, etc., was investigated on the performance of the thermal system.

Despite various advantages of solar air heaters, including low installation cost, simple configuration, negligible maintenance cost, and reduced fossil energy consumption, they have low thermal efficiency due to the low rate of heat transfer between the airflow and the heated surfaces. For this purpose, different active and passive heat transfer enhancement techniques have been widely developed for saving energy, optimal use of energy sources, increasing thermal efficiency, and reducing the size and cost of the system. Since the passive techniques are economical and further maintenance is not required, they have been widely used in solar air heaters. There are several experimental, theoretical, and numerical research works and published papers just to attack this issue in which some new thermal enhancement techniques have been proposed for increasing the system performance. An outstanding review of these research works was presented in a paper by Aravindh and Sreekumar [11].

Using fins, ribs, winglets, and obstacles can effectively increase the thermal performance of solar air heaters by increasing the area of heat transfer, disturbing the airflow, and increasing the convective heat transfer coefficient, which has been widely used by researchers [12-16]. Abdullah et al. [17] experimentally investigated the effect of turbulators on the performance of a double-pass solar air heater. The turbulators were cans attached to the upper and lower side of the absorber plate. The pressure drop, Nusselt number, and thermal efficiency were measured for aligned and staggered cans configurations and compared to the simple SAH. Esen [18] experimentally presented the exergy and energy analysis of a double-pass SAH in which various types of obstacles were placed on the absorber plate. The obtained results were presented and compared with and without obstacles. The exergy analysis based on the measurement of outlet air temperature and airflow rate showed that the thermal performance of the SAH was increased with obstacles. Akpinar and Kocyigit [19] experimentally investigated the effect of three different types of obstacles on the thermal performance of a flat-plate solar air heater. Using linear regression, some correlations were developed for the experimental measurements. The results showed that using obstacles can considerably improve the thermal efficiency of SAH. Sheikhnejad and Gandjalikhan Nassab [20] numerically investigated the flow pattern and thermal behavior of a solar air heater in which an elastic vortex generator was placed on the absorber plate to disturb the flow inside the boundary layer and increase the heat transfer coefficient and thermal performance of solar air heater.

Increasing the heat transfer area can effectively increase the thermal performance of solar air heaters as a passive thermal enhancement technique. For this purpose, double-pass solar air heaters have been developed in which the effective contact surface area between airflow and absorber plate is increased. Abo-Elfadl et al. [21] experimentally studied a double-pass solar air heater with a new design of an absorber, which was constructed from conductive aluminum tubes adjacent to each other. The measurements were carried out for various air flow rates. Moreover, the experimental results were compared to the results of a simple SAH with the same dimensions, which showed that higher efficiency and outlet air temperature as well as lower top heat loss was achieved. Alam and Kim [22] presented a comprehensive review of the thermal

enhancement strategies for double-pass solar air heaters. Three main techniques for performance improvement have been investigated both experimentally and numerically by the researchers, including increasing the convective heat transfer coefficients, decreasing the thermal losses, and increasing the heat transfer area. Hatami and Bahadorinejad [23] experimentally investigated the thermal performance of a flat-plate solar air heater in which the effect of one and two glass covers was studied. The thermal efficiency of six different cases of air heaters was analyzed, and a general relation for the Nusselt number was presented based on the Rayleigh number. The results showed that the maximum performance is obtained in the case of the double glass cover. Velmurugan and Kalaivanan [24] numerically studied a multi-pass flat-plate solar air heater from both the first and second laws of thermodynamic viewpoint. The results showed that the triple-pass SAH had the highest thermal performance compared to the single and double passes.

Using thermal storage and phase change materials (PCM) is another technique to improve the performance of single- and double-pass solar air heaters studied in the literature. Baig and Muhammad Ali [25] experimentally investigated a double-pass solar air heater in which the paraffin wax was used as the PCM integrated with porous aluminum metal. The experimental tests were carried out for different configurations during the winter season in which the effect of forced convection (using a fan) has been also taken into account. Mohamed Salih et al. [26] experimentally investigated a trapezoidal double-pass SAH with and without porous media. The experimental tests were carried out under free and forced convection airflow circulations. The results revealed that by using porous media, higher efficiency in both free and forced convection could be obtained. Sajawal et al. [27] experimentally studied the thermal performance of a double-pass solar air heater in which the metallic finned tubes of PCM were used as the thermal storage. The results of three different configurations with forced convection flow showed that optimum thermal performance could be obtained by using different PCMs in both passes.

However, a review of the literature shows that some innovative designs and structural variations can effectively increase the thermal performance of double-pass SAH. El-Said et al. [28] experimentally investigated the performance of a double-pass solar air heater in which the absorber plate was corrugated and a reflector was used to improve its hydraulic and thermal characteristics. The experimental analysis was carried out at different operating conditions, including various inclination angles and airflow rates. The results of the new design were compared with the conventional SAH, which revealed that a higher mass flow rate and a greater performance were obtained. Potgieter et al. [29] experimentally and numerically presented a new design for solar air heaters. Surface-to-surface radiation combined with a turbulence model was applied to numerically simulate the thermal behavior of the SAH, whose results were in good consistency with the experimental measurements. Moosavi et al. [30] presented a new and innovative design of a solar air heater combined with a windcatcher and a water spray system showing that the ventilation and performance could be increased significantly. Ozgen [31] experimentally studied a flat-plate double-pass solar air heater in which aluminum cans were placed inside the ducts as absorbers. Omojaro and Aldabbagh [32] experimentally studied the thermal performance of a single- and double-pass SAH with attached fins in which the absorber plate was made from a steel wire mesh, in which the thermal efficiency could be increased up to 20% compared to the single-pass SAH. Languri et al. [33] numerically studied a double-pass solar air heater in which a porous material was situated in the lower channel. The energy and exergy analysis was performed to obtain the optimum mass flow rate and maximum thermal efficiency of up to 30%. Mohamed Salih et al. [34] experimentally studied and compared natural and forced convection heat transfer in a double-pass solar air heater with a trapezoidal shape in winter weather, in which uniform fins were placed on both sides of the absorber plate. In the study by Hosseini et al. [35], many design aspects for enhancing convection heat transfer in terms of air temperature rise along naturally convecting SAHs were investigated. In order to increase the hydraulic performance of the solar air heater, Singh et al. [36] numerically analyzed a SAH with a tapered flow duct and bell-mouth

inlet opening. The results showed that the new design could significantly increase the mass flow rate and performance of the SAH. Mesgar Pour et al. [37] numerically studied a double-pass solar air heater with a helical flow path and triangular cross-section channel. The effect of different geometric parameters of this SAH on heat transfer performance was numerically investigated. Moreover, an optimization procedure by the differential evolution (DE) was carried out to obtain the maximum thermal performance, in which the triangular section angles, dimensions, and the location of the entrance section of each channel were considered as the design variables. Kalash et al. [38] experimentally and numerically investigated a double-pass solar air heater that was constructed from ten tubes. The thermal and hydraulic characteristics of three different configurations were examined during the daytime. Moreover, numerical simulations were carried out using computational fluid dynamics.

As the above review of the literature shows, many heat transfer enhancement techniques have been used to improve the thermal efficiency of solar air heaters. The double-pass solar air heaters with forced convection heat transfer and counter flow configuration were thoroughly studied in which some structural modifications such as using fins, cans, PCMs, and porous media could effectively improve the performance. However, passive thermal enhancement techniques in solar air heaters with natural flow regimes and parallel flow configuration, which are widely used for space heating, need to be more investigated, which is the main motivation of this study.

This paper aims to bridge the knowledge gap between the position effect of the absorber plate (as a passive thermal enhancement technique) and the thermal performance of the double-pass solar air heaters, which has not been addressed in the literature. The main contribution and novelty of this study compared with the previous studies of literature can be expressed as follows:

- Investigating the position effect of absorber plate as a passive thermal enhancement technique: Three different configurations of double-pass solar air heaters, in which the position of the absorber plate is changed, are simulated to investigate the hydraulic and thermal characteristics of SAH. Moreover, the obtained results are compared with each other and also with the single-pass SAH. The results show that the position of the absorber plate considerably affects the performance efficiency of the double-pass SAH.
- Investigating the performance of double-pass solar air heater: a 2-D transient set of transport governing equations is solved using commercial software COMSOL multi-physics to simulate the position effect of absorber plate on the performance of double-pass SAH, including airflow rate, air temperature, and thermal efficiency.
- Providing deep insight into the configuration of double-pass SAH: The position of the absorber plate has a double-edged sword impact on the outlet air temperature and airflow rate. The obtained numerical findings would provide good insight for the engineers, designers, and the scientific community in further developing efficient designs. The presented results can be used as a good reference to choose an alternative for the SAHs whether the criteria are the outlet temperature, airflow rate, or thermal efficiency.

Nomenclature

b	Height of air duct (m)
c_p	Specific heat (kJ/kg K)
L_1	Length of the horizontal duct(m)
g	Gravitational acceleration(m./s^2)
h	Convection coefficient (W/m^2K)
k_{th}	thermal conductivity ($Wm^{-1}K^{-1}$)
L	Length (m)
$\dot{m}$	Mass flow rate (kg/s)
n	Normal direction
Pr	Prandtl number
p	Pressure (Pa)
q''	Heat flux (W/m^2)
Ra	Rayleigh number
t	Time (s)
T	Temperature (K)
(u, v)	Velocity components (m/s)
(x, y)	Horizontal and vertical coordinates (m)

Greek symbols

α	Thermal diffusivity (m^2/s)
β	Volumetric thermal expansion (1/K)
κ	Turbulent kinetic energy (m^2/s^2)
δ	Thickness (m)
ε	Turbulence dissipation rate (m^2/s^3), Emissivity
τ	Transmissivity
μ	Dynamic viscosity (Pa.s)
ρ	Density (kg/m^3)

Subscript

a	Absorber
b	Bottom plate
amb	Ambient
g	Glass
t	Turbulent
o	Reference value
in	Inlet

Abbreviations

SAH	Solar air heater
PCM	phase change materials
RANS	Reynolds-Averaged Navier Stokes
FVM	Finite-Volume Method

2.Model description

The schematic of the solar air heater is presented in Fig. 1(a), whose components such as the absorber, the glass cover, the air duct, and the bottom plate are illustrated. The cold incoming air from the inlet section is passed through the duct to the outlet section due to the natural convection and buoyancy force. A constant solar heat flux is transmitted by the glass cover and reaches the thin absorber plate with high absorptivity. The outer surface of the glass cover is exposed to the ambient environment, for which an equivalent convection coefficient is considered as the boundary condition. The bottom plate is designed for absorbing the surface radiation from the absorber and converting more thermal radiation into gas enthalpy via convection heat transfer. The width and longitudinal length of the SAH duct are considered equal to L and L_1, respectively, while the cross-sectional height of the duct is equal to b, as seen in Fig. 1(b). Moreover, the values of all geometrical parameters and also some other information, including thickness (δ), thermal conductivity (κ), thermal diffusivity (α), transmissivity (τ), and temperature (T) are given in Table 1, in which the corresponding subscripts *a*, *b*, *g, in,* and *amb* indicate the absorber plate, bottom plate, glass cover, inlet, and ambient, respectively. It is worth noting that for the double-pass SAH, three different configurations are considered by changing the position of the absorber plate inside the main duct, as is shown in Fig. 2. In the first configuration, the absorber plate is placed near the glass cover on the upper third of the air duct, which is defined as case 1 and is shown in Fig. 2(a). Moreover, in the other two configurations, the absorber plate is placed in the middle and lower third of the air duct respectively, which are defined as case 1 and case 2 in Fig. 2(b) and Fig. 2(c), respectively.

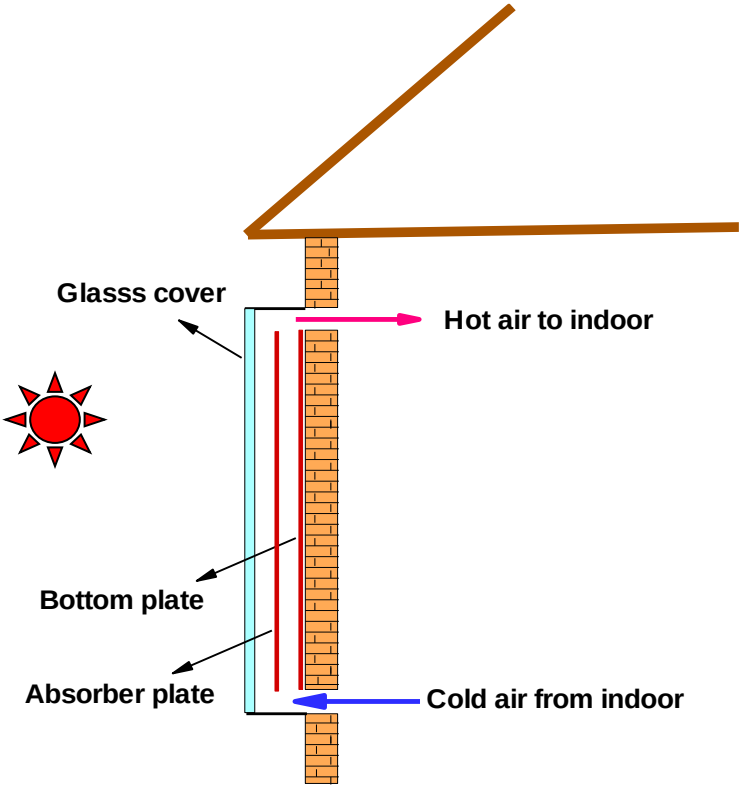

a) Schematic of SAH for space heating

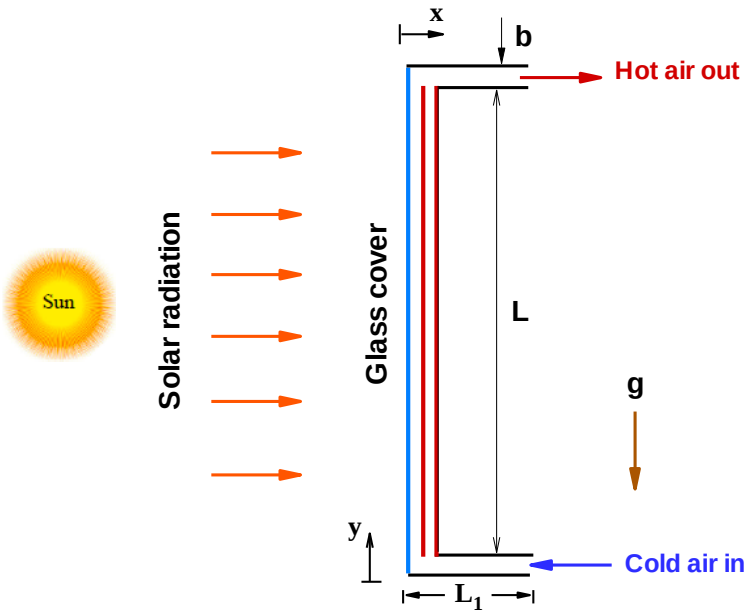

b) Details of SAH geometry for the simulation

Fig. 1. Geometry definition of SAH

Table 1. Values of the solar air heaters parameters

Parameter	Value	Parameter	Value
δ_g	4 mm	δ_a	2 mm
ε_g	0.9	ε_a	0.95
α_g	0.05	k_a	80 W/mK
τ_g	0.9	k_b	80 W/mK
k_g	0.78 W/mK	δ_b	2 mm
ε_b	0.95	T_{amb}	293 K
q''_{Sun}	400 W/m^2	T_{in}	293 K

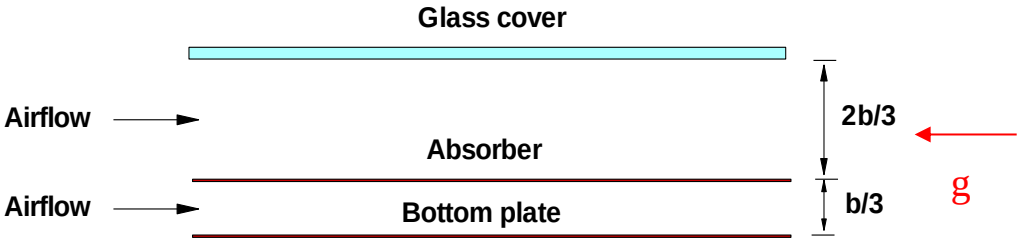

a) Case 1

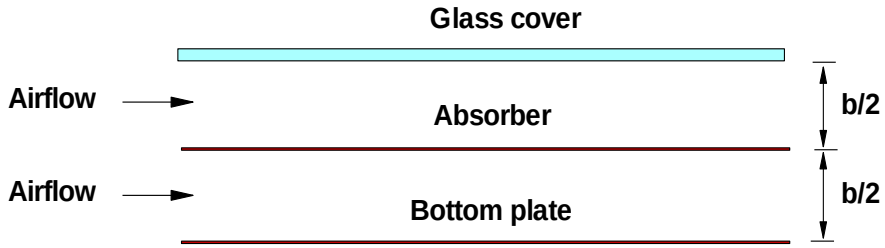

b) Case 2

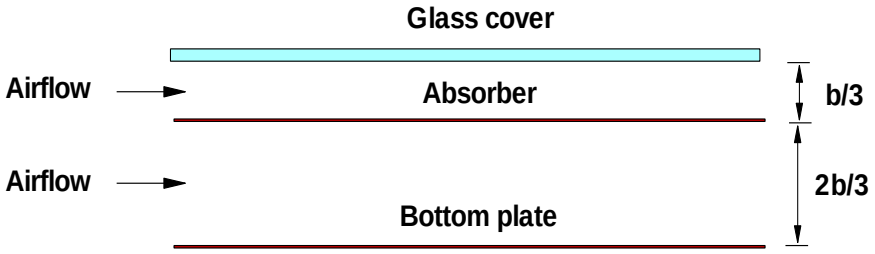

c) Case 3

Fig. 2. Three different configurations for the vertical duct of SAH

3.Theory

The fluid flow results from the balancing of two opposing forces, which are the buoyancy force due to the thermally induced density gradient, on the one hand, and the viscous and gravitational forces, on the other hand. The transient set of governing equations, including conservation of mass, momentum, and energy are presented as follows [39], in which the Boussinesq approximation has been implemented:

$$\nabla.V = 0 \tag{1}$$

$$\frac{\partial(\rho V)}{\partial t} + V.\nabla(\rho V) = -\nabla P + \nabla.\left[(\mu + \mu_t)\left(\nabla V + \nabla V^T\right)\right] + (\rho - \rho_o)g \tag{2}$$

$$\frac{\partial\left(\rho C_p T\right)}{\partial t} + V.\nabla\left(\rho C_p T\right) = \nabla.\left[\left(k_{th} + \frac{\mu_t}{Pr_t}\right)\nabla T\right] \tag{3}$$

$$\frac{\partial(\rho\kappa)}{\partial t} + V.\nabla(\rho\kappa) = \nabla.\left[\left[\mu + \frac{\mu_t}{\sigma_k}\right]\nabla k\right] + P_k + P_b - \rho\varepsilon + S_k \tag{4}$$

$$\frac{\partial(\rho\varepsilon)}{\partial t} + V.\nabla(\rho\varepsilon) = \nabla.\left[\left[\mu + \frac{\mu_t}{\sigma_\varepsilon}\right]\nabla\varepsilon\right] + C_1\frac{\varepsilon}{k}(P_k + C_3P_b) - C_2\rho\frac{\varepsilon^2}{k} + S_\varepsilon \tag{5}$$

where, $\mu_t = C_\mu\frac{\rho k^2}{\varepsilon}$ is the turbulent viscosity, P_k and P_b denote turbulent and buoyancy production, while C_1, C_2, C_3 are constants. Moreover, the input and initial parameters are presented in Table 2, while more details can be found in Ref. [39]. Moreover, the temperature dependency of all thermo-physical properties has been taken into account for the airflow, while the Boussinesq approximation is employed to consider the buoyancy effect. The well-known standard $k-\varepsilon$ model [39] is implemented to simulate the turbulent nature of convective flow based on the RANS problem. It is worthwhile noting that since the value of Rayleigh number ($Ra = g\rho\beta q'' b^4/k\mu\alpha$) is in order of 10^9, the turbulence regime is considered for the natural fluid flow [40].

In temperature computations of solid elements, the absorbed solar radiation by the absorber with an opaque surface is modeled by applying constant heat flux as a boundary condition, while the absorbed solar radiation inside the transparent glass cover is employed as a source term in the conduction equation. Thereby, the following partial differential equations are considered for temperature computations of the glass sheet, the absorber, and the bottom plates:

$$\frac{\partial^2 T}{\partial x^2} + \frac{\partial^2 T}{\partial y^2} + \frac{q_{Sun}.\alpha_g}{k_g.\delta_g} = \frac{1}{\alpha}\frac{\partial T}{\partial t} \tag{6}$$

$$\frac{\partial^2 T}{\partial x^2} + \frac{\partial^2 T}{\partial y^2} = \frac{1}{\alpha}\frac{\partial T}{\partial t}. \tag{7}$$

3.1.Initial and boundary conditions

The set of governing equations is solved simultaneously in a transient condition by marching in time. Also, the turbulent $\kappa-\varepsilon$ model is applied to obtain the turbulent stress and heat fluxes. Initial and boundary conditions are considered as follows:

- There is no airflow at the initial time ($t = 0$), and it is supposed to be stagnant. Moreover, the temperature of all solid parts and the working gas is the same as the room temperature of 293 K.
- Regarding pressure boundary conditions at the inlet and outlet duct sections, the ambient pressure is imposed (zero gauge pressure).
- The convection boundary condition with its equivalent convection coefficient on the glass surface adjacent to the surrounding with T_{amb}=288 K was employed. Moreover, the convective and .radiative parts of the equivalent coefficient of heat transfer are calculated based on the following expressions [41]:

$$h_{\text{conv}} = 5.7 + 3.8V_{\text{wind}} \quad \text{and} \tag{8}$$

$$h_{\text{rad}} = \sigma\varepsilon_g\left(\frac{T_g^4 - T_{\text{sky}}^4}{T_g - T_{\text{amb}}}\right), \tag{9}$$

where the sky temperature is approximated as

$$T_{\text{sky}} = 0.0522T_{\text{amb}}^4. \tag{10}$$

- Because of insulation, the outer surface of the bottom plate is considered to be adiabatic.
- On the absorber surface, a constant heat flux equal to ($\tau_{\text{glass}} \times q_{\text{Sun}}$) is assigned.

- In the surface radiation computations, the glass, absorber, and bottom plates are considered to be gray with constant emissivity. Also, the absorber and bottom plates are assigned opaque bodies.
- For the interfaces between the airflow and solid elements, the following conjugate heat transfer boundary conditions (continuity of heat flux and temperature) are considered:

$$(k\frac{\partial T}{\partial n})_{\text{solid}} = (k\frac{\partial T}{\partial n})_{\text{air}} \tag{11}$$

$$T_{\text{solid}} = T_{\text{air}} \tag{12}$$

3.2.Numerical scheme

The computational domain is discretized by applying the finite-element method (FEM), and the numerical solution of the governing equations is obtained by employing the commercial software COMSOL multi-physics. The structured orthogonal grids with 24500 cells are used with clustering near the boundaries where the gradients of dependent variables are significant. This optimum grid size is obtained by a comprehensive grid-independency study, such that a 10% increase in the number of grids yields less than 2% variation in the computed value of the maximum temperature on the absorber surface as the most sensitive dependent variable to the size of the grid. The schematic of grid generation inside the solution domain is depicted in Fig. 3. Moreover, the results of grid dependency are tabulated in Table 3. Moreover, since the transient numerical simulation is considered, in addition to the spatial grid size, the time step has a significant impact on the accuracy of simulation results. For this purpose, the simulation has been carried out for different values of time steps, and the maximum time step of 0.006 seconds has been distinguished as the optimum time step. Moreover, in the numerical simulation, the convergence criteria are considered to be equal to 1×10^{-4} for the temperature field and 2×10^{-4} for the velocity field, turbulent kinetic energy, and its dissipation rate for the converged solution at each time step. It should be mentioned that as the wall function is considered in velocity computations near the walls, the minimum value of y^+ is maintained about 35, which has been considered in grid generation [42]. The flowchart of the numerical procedure is presented in Fig. 4.

Table 2. Summary of methodology

Flow regime	Flow modeling method.	Algorithm of solution	Rayleigh No.	Reynolds No.
Turbulent	Standard $k-\varepsilon$	SIMPLE	10^9	3000
C_1	C_2	C_3	σ_ϵ	σ_k
1.44	1.92	0.09	1.3	1.0

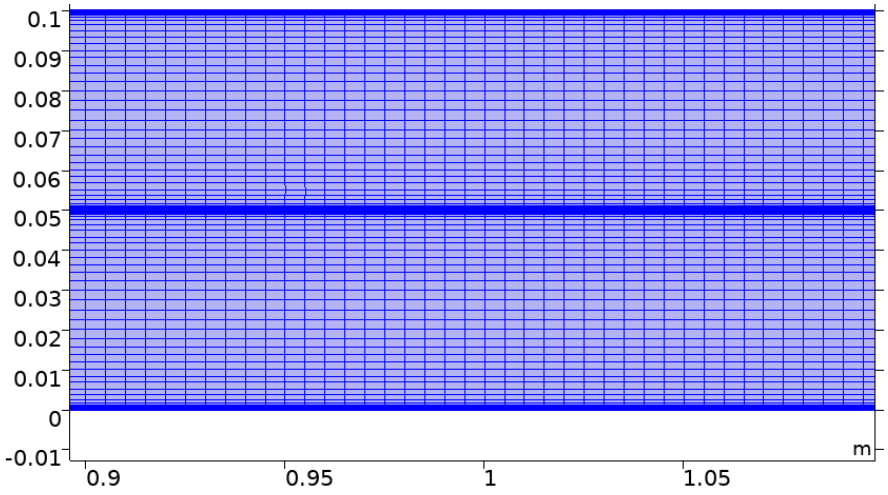

Fig. 3. Schematic of grid nodes inside a portion of vertical duct ($0.9\ m \le y \le 1.1\ m$)

Table 3. Comparison of maximum temperature at different grid sizes

Number of grids	7800	11300	15400	19800	24500	29600
T_{max} (K)	325.9	350.7	370.2	381.2	386.4	388.3
Error with respect to the previous step	-	7.6%	5.7%	3%	1.3%	0.4%

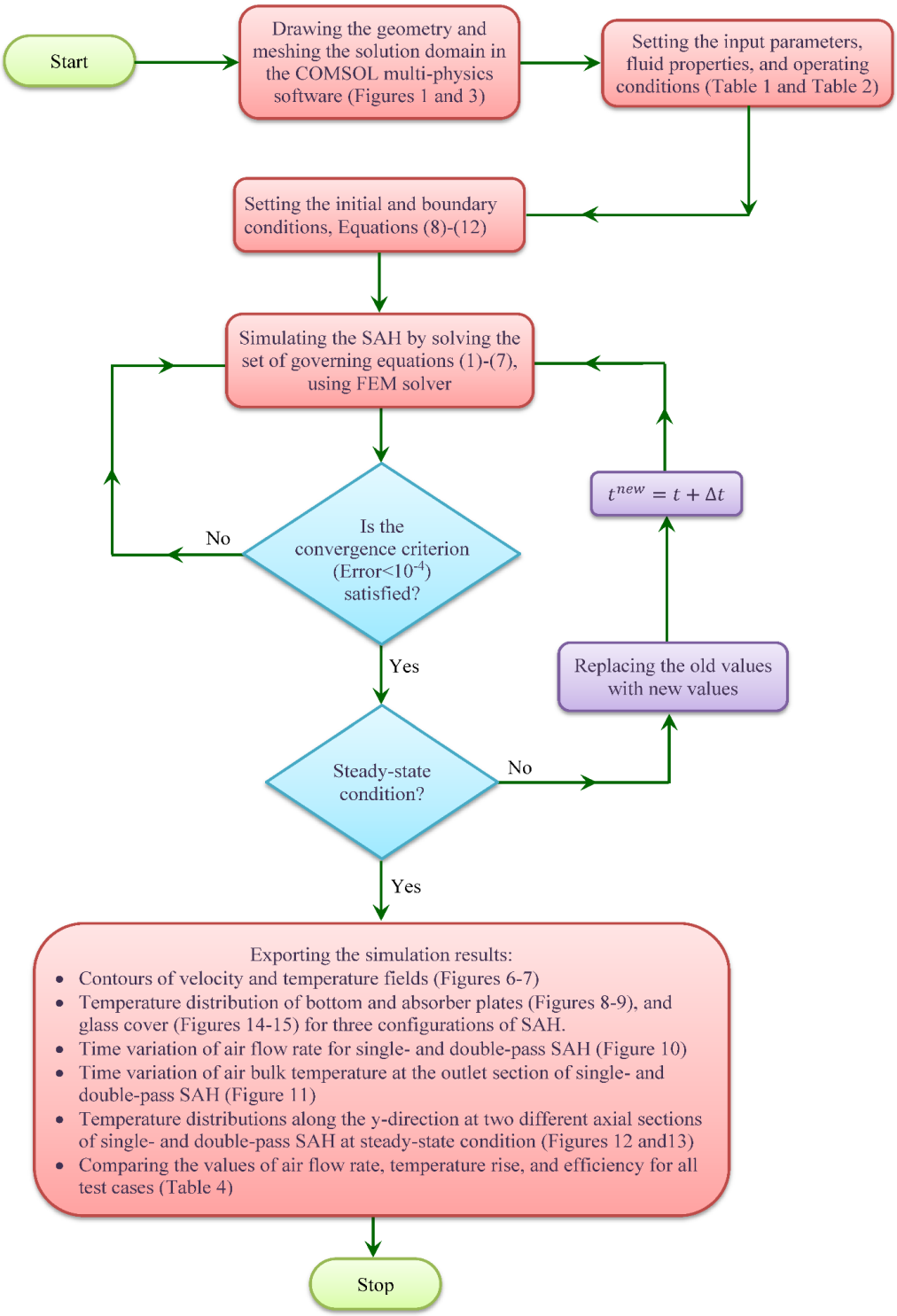

Fig. 4. Flowchart of the numerical procedure

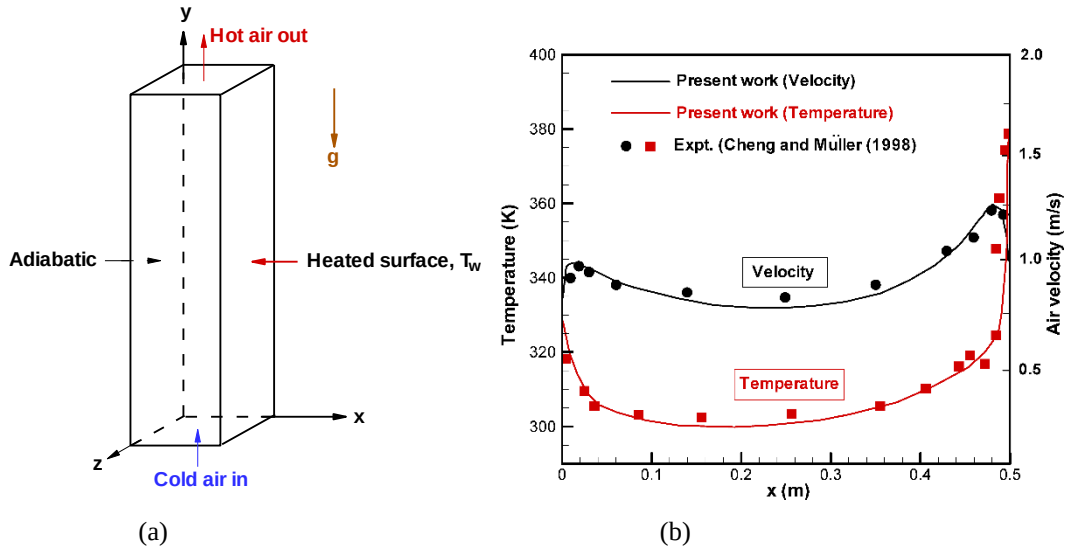

(a) (b)

Fig. 5. Schematic of the simulated chimney: a) Temperature and velocity distributions across the channel at y=7.8 m, and b) comparison with experiment [42].

4.Validation

In order to validate the numerical method, a test case has been simulated in which natural convection heat transfer of airflow in a vertical channel is simulated. The channel is long with heated walls, which is similar to the geometry of the present study. This test case has been experimentally studied by Cheng and Muller [42]. The vertical channel has a square cross-section area of 0.5×0.5 m, while its height is equal to 8 m. Since the top and bottom surfaces are considered to be adiabatic, a two-dimensional model can be regarded as a reasonable assumption. For this purpose, a 2D simulation is carried out at the mid-plane ($z = L_z/2$).

The heated wall is considered to be kept at a constant temperature of 423 K, while the adiabatic boundary condition is considered for the other wall. Moreover, the natural convective flow is considered to be turbulent with the Rayleigh number equal to 5×10^{12}. In Fig. 5, the variations of velocity and temperature at the steady-state condition and y=7.8 m are presented and compared with the experimental measurements. As it is clearly observed, the obtained numerical results match well with the extracted experimental data (with a maximum error of 1.5 %), which confirms the validity of the present numerical method in the simulation of natural convective flow in SAHs.

5.Results and discussion

The simulation results for comprehensive hydraulic and thermal analysis of transient turbulent natural convection in a solar air heater for space heating are presented in this section. At first, the evolution of air velocity along the chimney at the steady-state condition is demonstrated in Fig. 6. It shows how the flow field evolves in both single- and double-pass SAHs. Also, in double-pass heaters, three different locations of the absorber are considered in cases 1 to 3. It is worth noting that the numerical simulation has been carried out from $t = 0$ s to $t = 4000$ s, after which the steady-state condition is achieved. At the initial time, the transmitted solar radiative by the glass cover reaches the absorber plate and is absorbed due to the high absorptivity. Since the absorber plate is heated up, a significant temperature gradient is created between the heated absorber surface and its adjacent air, which causes a great force to drive the air as fast as possible. The velocity magnitude contours in Fig. 6 depict that due to the buoyancy effect, the air flows with high velocity near the heated surface throughout the duct from the inlet toward the outlet section. In the double-pass SAHs, the existence of an absorber plate has two opposite effects on the airflow rate inside the chimney as the main desired parameter. On the one hand, as the free convection airflow passes from both the upper

and lower surfaces of the heated absorber, the area of convective heat transfer is increased, and the two high-velocity regions adjacent to the heated surface lead to more airflow rate inside the chimney. On the other hand, the viscosity effect in both upper and lower boundary layers has an opposite effect on the airflow rate. However, Fig. 6 shows similar flow patterns inside the single and double pass types with recirculated zones adjacent to the corners.

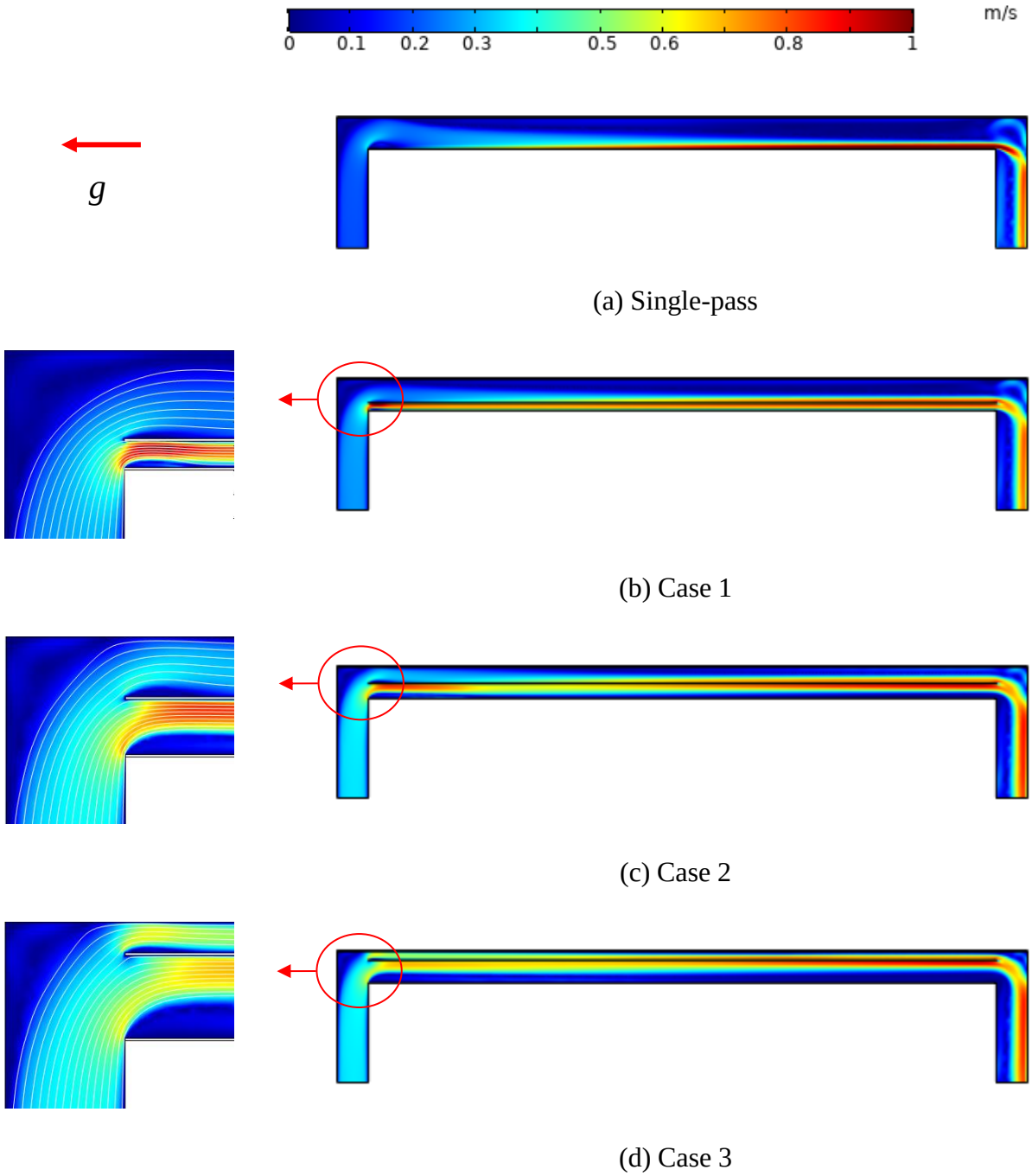

Fig. 6. Velocity magnitude contours

The temperature contour plots inside the single- and double-pass SAHs are shown in Fig. 7, respectively. These figures show how the free convective airflow is heated via convection heat transfer by the absorber and bottom plates. Fig. 7 depicts that the major part of energy conversion from thermal radiation into the gas enthalpy in double-pass SAH takes place in the upper pass because the maximum temperature occurs on the absorber top surface, which is under the incidence of incoming solar radiation. Because of the low air conductivity, the depth of heat penetration from the heated absorber plate into the upper and lower convective air flows is still small, but it is more than the heat penetration depth in single-pass SAH. On the other hand, it should be recalled that the existence of a large heat transfer surface area between the absorber plate and working gas in double-pass heaters causes a temperature decrease on the heated surface, which leads to a more reversible heat transfer process. Thereby, the absorber plate in single-pass SAH is at a higher temperature in comparison with double-pass SAH, in which the absorber is in contact via its upper and lower surfaces with convective air flows.

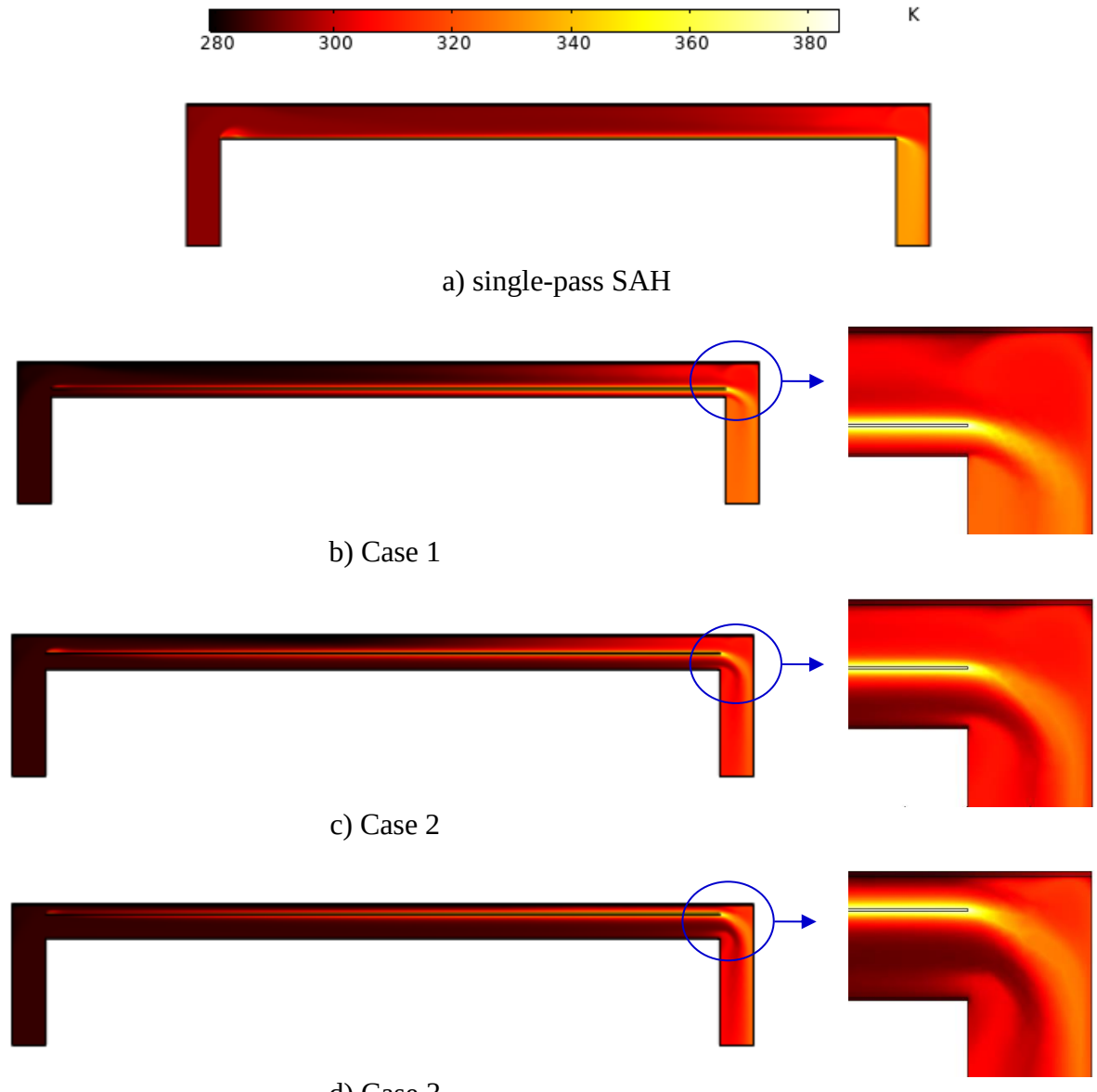

a) single-pass SAH

b) Case 1

c) Case 2

d) Case 3

Fig. 7. Temperature contours in single- and double-pass SAH

To study more about the thermal behavior of SAH in the transient period, the absorber temperature distribution along its length in single-pass SAH is plotted in Fig. 8 for four different times, including the steady-state condition (t=4000 s). For all different times, the absorber temperature has an increasing trend along the flow direction, which is due to the growth of the thermal boundary. Moreover, as expected, the maximum temperature occurs at the steady-state condition, and the end of the absorber with $T_{max} = 112$ ℃.

The temperature distributions along the absorber and bottom plate of double-pass SAH are plotted in Fig. 9 at the steady-state condition. The temperature increase in flow direction is observed again similar to the single-pass one, which is due to the growths of the thermal boundary layer thickness, such that the absorber temperature for all three cases remains almost the same, but the bottom plate has its maximum temperature for case 1, in which there is a narrow gap between this plate and absorber. This factor damps the convection heat transfer and leads to a higher temperature of the heated surface. If one compares the temperature distributions along the absorber and bottom plates, it can be found that the major part of energy conversion from solar irradiation into air enthalpy takes place by the absorber, such that the bottom plate doesn't play an important role in this process. One of the important findings from Fig. 9 is the high rate of absorber temperature increase along the flow direction, which is due to the resistance of the thermal boundary layer that has a negative effect on the performance of the solar heater. So, it will be expected that SAHs with short ducts have higher performances in generating high-temperature air flows.

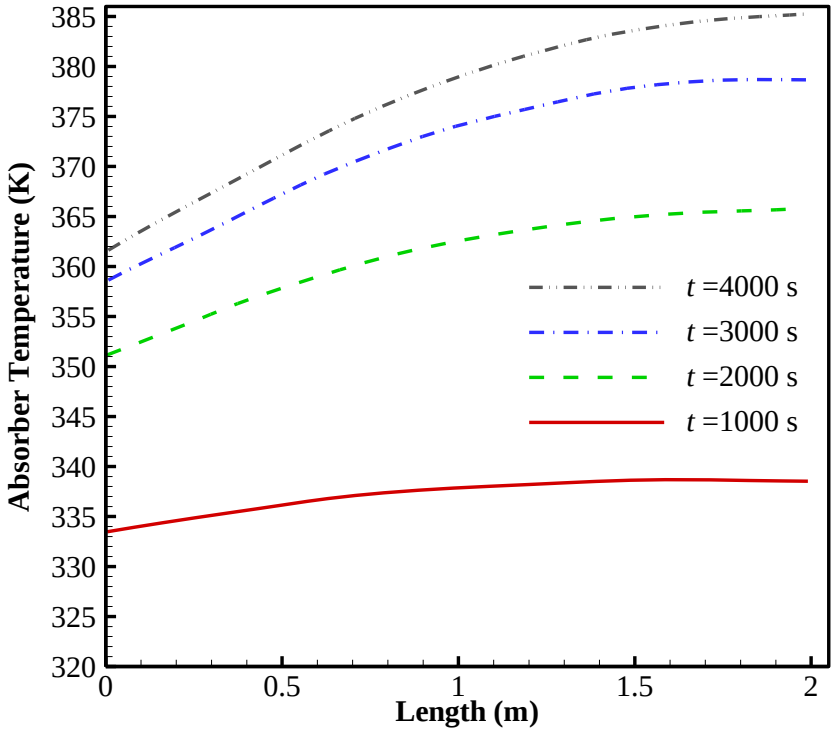

Fig. 8. Absorber temperature for single-pass SAH at different time

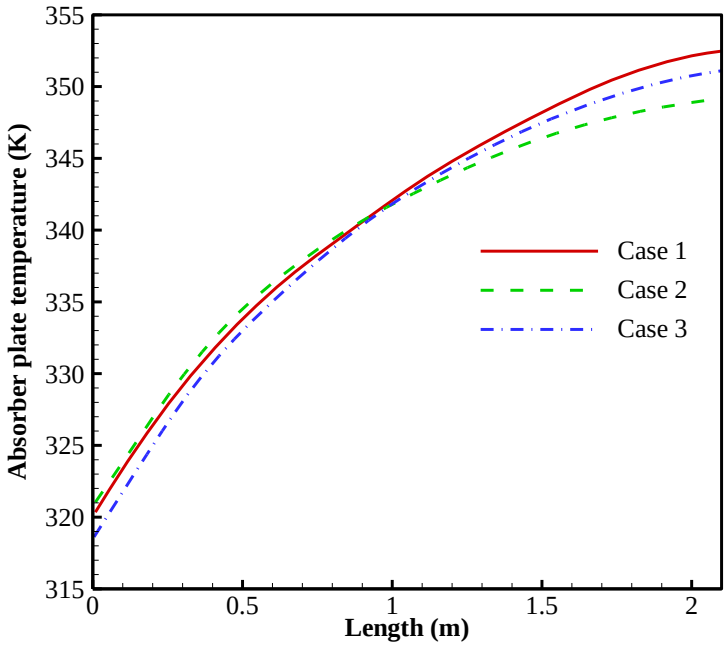

a) Absorber

b)

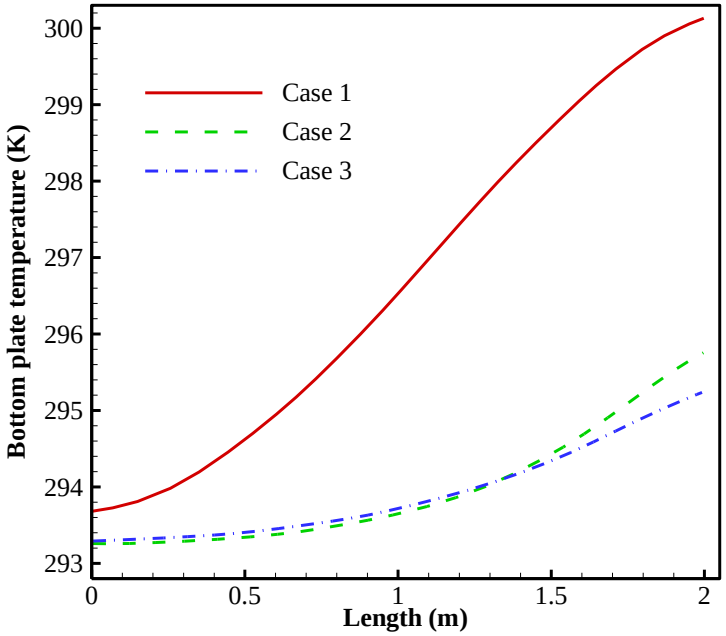

c) Bottom plate

Fig. 9. Absorber and bottom plate temperature distributions for three cases at steady-state condition

One of the main parameters that significantly affects the performance of SAHs is the airflow rate. As was mentioned before, the transmitted solar radiative flux heats the absorber plate in a way that a significant temperature gradient is created between the surface and its adjacent air, which causes a great force to drive the air as fast as possible. This phenomenon can be seen in Fig. 10, which shows the time history of the volumetric airflow rate through both single- and

double-pass SAHs. Comparison between the curves plotted in this figure indicates that the airflow rate in double-pass SAH is much higher than that of single-pass, especially for case 3. The amount of airflow rate, in this case, is about two times of single-pass SAH. So, this case can be a good choice for more ventilation which induces more fresh air into the space in comparison with the other cases as well as with single-pass SAH. However, it is evident that the outlet temperature for case 3 must be less than others because of energy conservation.

To better elaborate on the thermal performance of SAH, the time histories of outlet bulk temperatures for all of the test cases are plotted in Fig. 11. The maximum outlet temperature belongs to the single-pass SAH with T_{out} = 327 K. Among the three cases studied for the double-pass type, the outlet temperature in case 1 is the highest (T_{out} = 317.5 K), and the minimum one takes place in case 3 (T_{out} = 312 K) as was expected before.

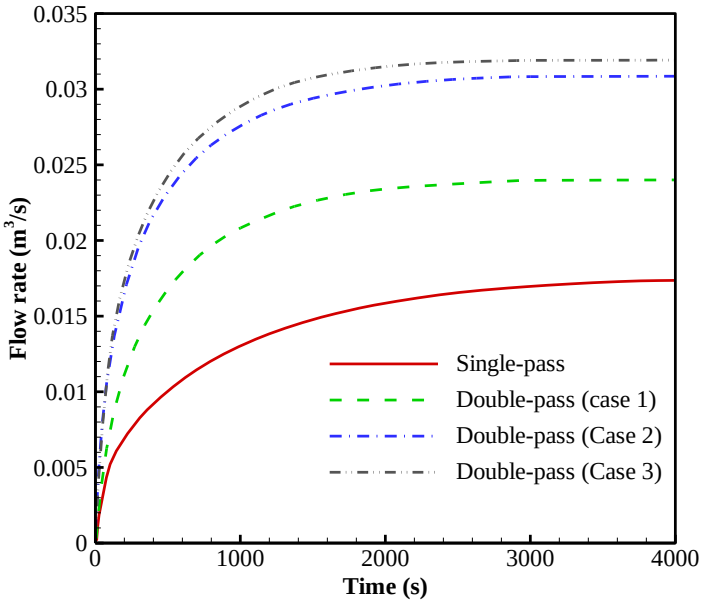

Fig. 10. Time history of air flow rate in single- and double-pass SAH

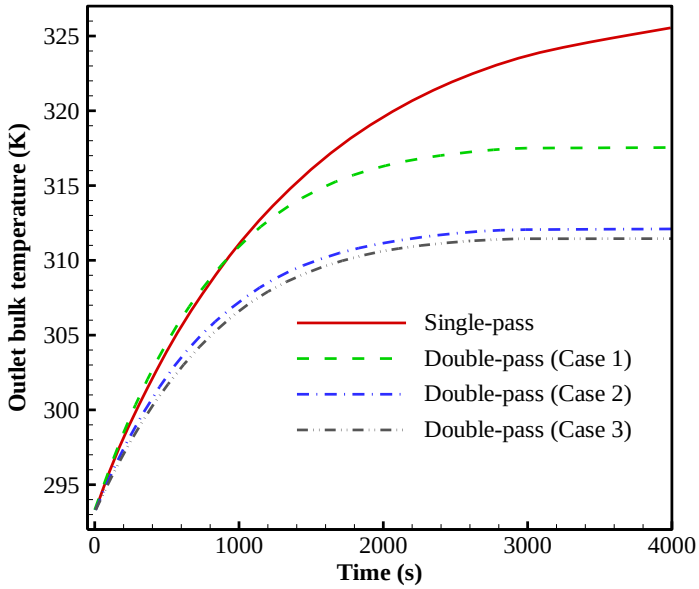

Fig. 11. Time history of the air bulk temperature at the outlet section of single- and double-pass SAH

To better demonstrate the thermal behavior of SAHs, the temperature distribution across the main duct of SAHs at two different axial sections is plotted in Figs. 12 and 13. It is seen from Fig. 12 that the penetration of thermal energy from the heated absorber into convective airflow mainly happens in a thin layer of air near the heated surface due to the poor convection coefficient. This defection is almost compensated in double-pass SAHs by increasing the surface area and dividing the convective airflow into two passes. In all test cases, the maximum temperature occurs at the absorber and the minimum one on the glass cover. As is seen in Fig. 13, the trends of temperature variation across the axial air duct section are almost identical for all of the cases. Another point worth mentioning is that although the bottom plate is under the incidence of emitted radiative energy from the absorber by surface radiation, it does not have a considerable role in heating the airflow by convection heat transfer.

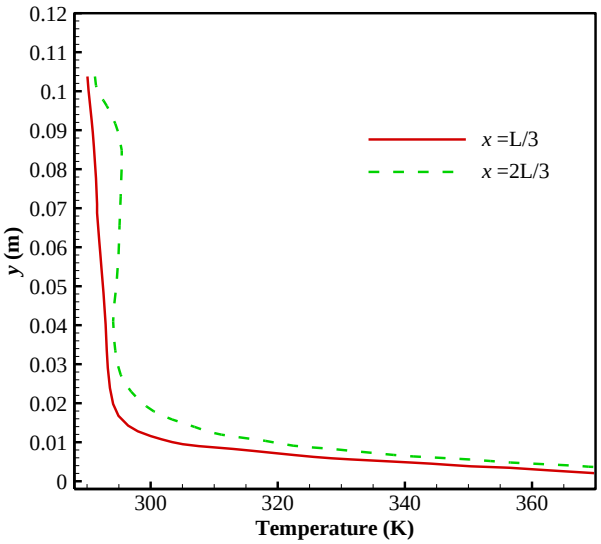

Fig. 12. Temperature distributions along the y-direction at two different axial sections of single-pass SAH at steady-state condition

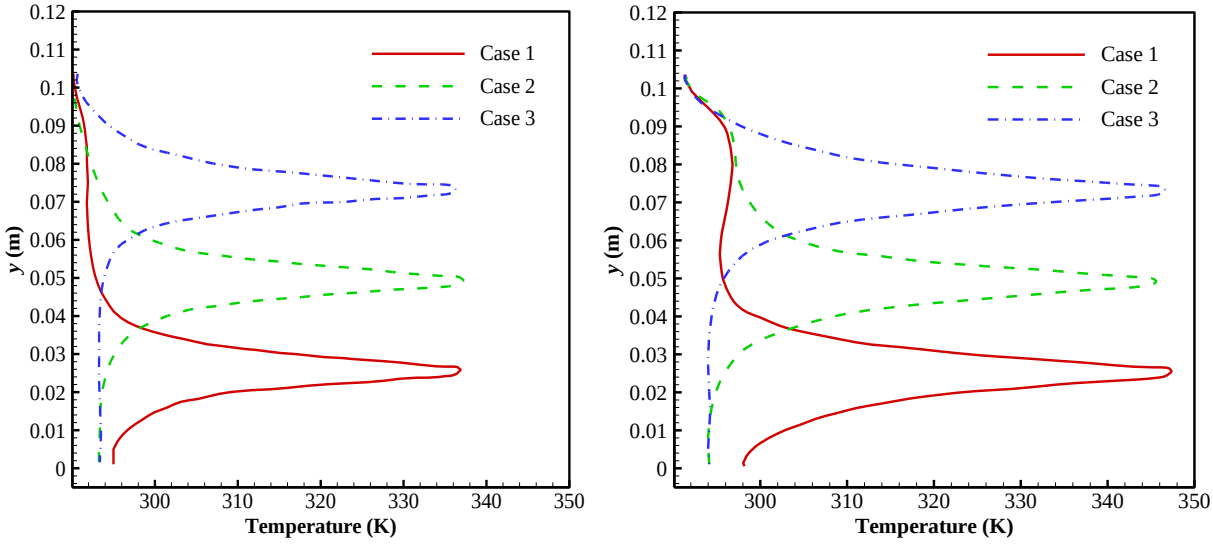

a) x=L/3 b) x=2L/3

Fig. 13. Temperature distributions along the y-direction at two different axial sections of double-pass SAH at steady-state condition

Since the only heat loss from the SAH into the surrounding takes place from the glass cover, the surface temperature distributions of the glass cover for all of the test cases are depicted in Fig. 14 and 15 for better illustration. These figures show relatively low glass temperature because this element is in heat transfer with the ambient air, which is considered to be at T=288 K, corresponding to the cold air in the winter. But the difference between the average glass temperature and ambient temperature is not too high, revealing a low rate of heat loss from this element. However, the glass temperature distribution for all test cases has a similar trend so that the maximum temperature occurs at the end of the channel with the maximum value of 301 K in case 3 of double-pass SAHs. So, a high value of thermal efficiency can be predicted for these types of SAHs, which is defined as follows:

$$\eta = \frac{\dot{m}C_p\left(T_{out} - T_{in}\right)}{q^{''}_{Sun}.A} \tag{13}$$

The values of thermal efficiency, airflow rate, and temperature rise along the heaters for all test cases are tabulated in Table 4. As it is seen, relatively high thermal efficiencies are predicted for double-pass types of solar air heaters, such that the maximum efficiency belongs to case 3 of double-pass SAHs, which is about 78%. So, Table 4 can be a good reference for choosing a good alternative for SAHs, whether the criteria are the outlet temperature, airflow rate, or thermal efficiency.

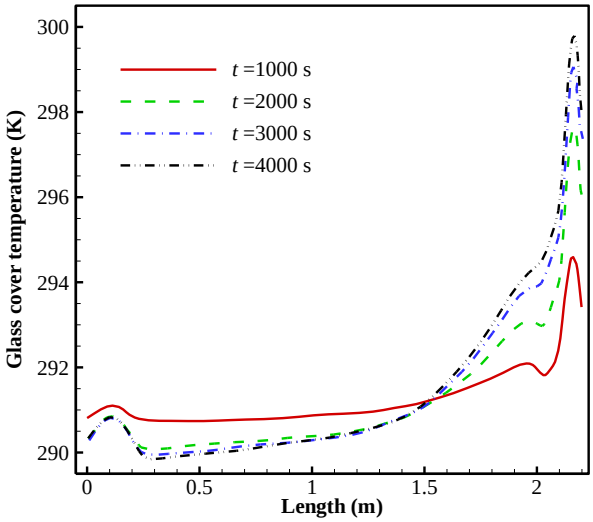

Fig. 14. Time history of glass surface temperature distribution for single-pass SAH

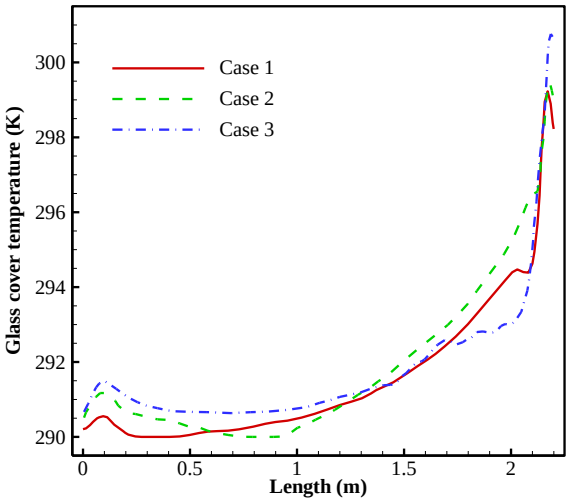

Fig. 15. Glass surface temperature distribution for double-pass SAH at steady-state condition

Table 4. The values of air flow rate, temperature rise, and efficiency for all test cases

Test cases		Air flow rate (m^3/s) × 10^3	Temperature rise (K)	Efficiency (%)
Single-pass SAH		17	32	68
Double-pass SAH	Case 1	24	25	75
	Case 2	31	19.5	75
	Case 3	33	19	78

6.Conclusion

In the present study, the thermal-hydraulic performance of a single- and double-pass solar air heater with turbulent natural air flow is thoroughly investigated as a sustainable solution for space heating. The position effect of the absorption plate on the thermal performance of a double-pass solar air heater has been highlighted as the main contribution of this study. For this purpose, the set of governing equations, including the conservations of mass, momentum, and energy were solved simultaneously to simulate the transient behavior of SAH. Numerical calculations were carried out using the finite-element method (FVM), while the well-known standard κ- ε turbulent model was employed to simulate the turbulent natural convection airflow. Also, the conduction equation was solved for obtaining the temperature fields in the solid elements, including the glass cover, absorber, and bottom plate. The set of governing equations was solved simultaneously using the commercial software COMSOL multi-physics to simulate the thermal-hydraulic performance of the SAH at the transient period and steady-state conditions. The results of temperature and airflow fields in three different configurations of double-pass solar air heaters with natural airflow are comprehensively investigated and compared with a single-pass SAH. The obtained numerical results are summarized as follows:

- The results revealed that the position of the absorber plate considerably affects the thermal and hydraulic behavior and performance efficiency of the double-pass SAH. Moreover, in both single- and double-pass SAHs, the absorber plate temperature is an increasing function of its length in the flow direction.
- The position of the absorber plate has a double-edged sword impact on the outlet air temperature and airflow rate.
- In the double-pass solar air heater, since both the upper and lower surfaces of the absorber plate are heated, the total convective heat transfer area is increased, and the two high-velocity regions adjacent to the heated surface lead to more airflow rate inside the chimney compared to the single-pass SAH.
- In the double-pass SAH, as the absorber plate approaches the glass cover (case 3), the airflow rate increases significantly in a way that its value is two times greater than the airflow rate in the single-pass SAH (an increase of 100% in airflow rate).
- Unlike the flow rate, among the three cases of double-pass SAH, the minimum outlet air temperature is observed in case 3 ($T_{out} = 312\ K$), in which the absorber plate is near the bottom wall. Moreover, the maximum outlet temperature belongs to the single-pass SAH with $T_{out} = 327\ K$.
- The performance analysis of all cases shows that double-pass SAHs generally have higher thermal efficiencies compared to the single-pass SAH with $\eta = 68\%$. Moreover, among the three configurations of double-pass SAHs, maximum thermal efficiency belongs to case 3 with $\eta = 78\%$, which shows that a 15% improvement can be achieved by changing the position of the solar absorber.
- The presented results can be used as a good reference for choosing a good alternative for the SAHs whether the criteria are the outlet temperature, airflow rate, or thermal efficiency.

Declaration of interest statement

The authors declare that they have no known competing financial interests or personal relationships that could have appeared to influence the work reported in this paper.

References

[1] Gill, R.S., Singh, S., Singh, P.P., Low cost solar air heater, Energy Conversion and Managements (2012) 57: 131-142.

[2] Tuncer, A.D., Khanlari, A., Sözen, A., Gürbüz, E.Y., Şirin, C., Gungor, A., Energy-exergy and enviro-economic survey of solar air heaters with various air channel modifications, Renewable Energy (2020) 160: 67-85.

[3] Sudhakar, P., Cheralathan, M., Thermal performance enhancement of solar air collector using a novel V-groove absorber plate with pin-fins for drying agricultural products: an experimental study, Journal of Thermal Analysis and Calorimetry, (2020) 140: 2397-2408.

[4] Raj, A. K., Kunal, G., Srinivas, M., Jayaraj, S., (2019) Performance analysis of a double-pass solar air heater system with asymmetric channel flow passages, Journal of Thermal Analysis and Calorimetry, 136: 21–38.

[5] M. Foruzan Nia, S.A. Gandjalikhan Nassab, A.B. Ansari, Numerical Simulation of Flow and Thermal Behavior of Radiating Gas Flow in Plane Solar Heaters. Journal of Thermal Science and Engineering Applications (2020) 12: 031008.

[6] Gandjalikhan Nassab, S. A., Moein Addini, M. Heat transfer enhancement in solar air heater with turbulent natural convection by two flapping elastic winglets, Energy Equipment and Systems (2021) 19:3 209-227.

[7] Palaniappan, C., Subramanian, S.V., Economics of solar air pre-heating in south Indian tea factories: a case study, Solar Energy (1998) 63:1, 31-37.

[8] Sachdev. T., Gaba, V. K., Tiwari, A. K., Performance analysis of desalination system working on humidification-dehumidification coupled with solar assisted air heater and wind tower: Closed and open water cycle, Solar Energy (2020) 205: 254-262.

[9] Choudhury, P.K., Baruah, D.C., Solar air heater for residential space heating. Energy, Ecology Environment (2017) 2:6 387-403.

[10] Shi, L., Zhang, G., Cheng, X., Guo, Y., Wang, J., Lin Chew, M.Y., Developing an empirical model for roof solar chimney based on experimental data from various test rigs. Building and Environment (2016) 110: 115-128.

[11] Aravindh, M. A., Sreekumar, A., Efficiency enhancement in solar air heaters by modification of absorber plate-a review. International Journal of Green Energy, (2016) 13:12, 1209-1223.

[12] Chamoli, S., Thakur, N. S., Exergetic performance evaluation of solar air heater having V-down perforated baffles on the absorber plate. Journal of Thermal Analysis and Calorimetry, (2014) 117: 909-923.

[13] Gholami, A., Ajabshirchi, Y., Ranjbar, S., F., Thermo-economic optimization of solar air heaters with arcuate-shaped obstacles Journal of Thermal Analysis and Calorimetry, (2019) 138: 1395-1403.

[14] Bhattacharyya, S., The effects of short length and full length swirl generators on heat transfer and flow fields in a solar air heater tube. Journal of Thermal Analysis and Calorimetry, (2020) 140: 1355-1369.

[15] Bhattacharyya, S., Pathak, M., Sharifpur, M., Chamoli, S., Ewim, D. R. E., Heat transfer and exergy analysis of solar air heater tube with helical corrugation and perforated circular disc inserts. Journal of Thermal Analysis and Calorimetry, (2021) 145: 1019-1034.

[16] Skullong, S., Kwankaomeng, S., Thianpong, C., Promvonge, P., Thermal performance of turbulent flow in a solar air heater channel with rib-groove turbulators, International Communication in Heat and Mass Transfer (2014) 50: 34-43.

[17] Abdullah, A.S., Al-sood, M.M.A., Omara, Z.M., Bek, M.A., Kabeel, A.E., Performance evaluation of a new counter flow double pass solar air heater with turbulators, Solar Energy, (2018) 173: 398-406.

[18] Esen, H., Experimental energy and exergy analysis of a double-flow solar air heater having different obstacles on absorber plates, Building and Environment (2008) 43, 1046-1054

[19] Akpinar, E.K., Koçyiğit, F., Experimental investigation of thermal performance of solar air heater having different obstacles on absorber plates, International Communication in Heat and Mass Transfer, (2010) 37: 416-421.

[20] Sheikhnejad. Y., Gandjalikhan Nassab. S.A., Enhancement of solar chimney performance by passive vortex generation, Renewable Energy (2021) 169: 437-450.

[21] Abo-Elfadl, S., Hassan, H., El-Dosoky, M.F. (2020) Study of the performance of double pass solar air heater of a newly designed absorber: An experimental work, Solar Energy, 198: 479-489.

[22] Alam, T., Kim, M. H. Performance improvement of double-pass solar air heater – A state of the art of review, Renewable and Sustainable Energy Reviews (2017) 79: 779-793.

[23] Hatami, N., Bahadorinejad, M., Experimental determination of natural convection heat transfer coefficient in a vertical flat-plate solar air heater, Solar Energy, (2008) 82: 903-910.

[24] Velmurugan, P. Kalaivanan, R., Energy and Exergy Analysis of Multi-Pass Flat Plate Solar Air Heater-An Analytical Approach, International Journal of Green Energy, (2015) 12:8, 810-820.

[25] Baig, W., Muhammad Ali, H. An experimental investigation of performance of a double pass solar air heater with foam aluminum thermal storage medium. Case Studies in Thermal Engineering (2019) 14: 100440.

[26] Mohamed Salih, M. M., Alomar, O. R., Yassien, H. N. S., Impacts of adding porous media on performance of double-pass solar air heater under natural and forced air circulation processes, International Journal of Mechanical Sciences, (2021) 210: 106738.

[27] Sajawal, M., Rehman, T., Muhammad Ali, H., Sajjad, U., Raza, A., Bhatti, M.S. Experimental thermal performance analysis of finned tube-phase change material based double pass solar air heater, Case Studies in Thermal Engineering (2019) 15: 100543.

[28] El-Said, E.M.S., Gohar, M.A., Ali, A., Abdelaziz, G.B., (2022) Performance Enhancement of a Double Pass Solar Air Heater by Using Curved Reflector: Experimental Investigation, Applied Thermal Engineering, 202: 117867.

[29] Potgieter, M.S.W., Bester, C.R., Bhamjee, M., Experimental and CFD investigation of a hybrid solar air heater, Solar Energy (2020) 195: 413-428.

[30] Moosavi, L., Zandi, M., Bidi, M., Behroozizad, E., Kazemi, I., New design for solar chimney with integrated windcatcher for space cooling and ventilation. Building and Environment (2020) 181: 106785.

[31] Ozgen, F., Esen, M., Esen, H., Experimental investigation of thermal performance of a double-flow solar air heater having aluminum cans. Renewable Energy (2009) 34: 2391-2398.

[32] Omojaro, A.P., Aldabbagh, L.B.Y., Experimental performance of single and double pass solar air heater with fins and steel wire mesh as absorber, Applied Energy (2010) 87: 3759-3765.

[33] Languri, E. M., Taherian, H., Hooman, K., Reisel, J., Enhanced Double-Pass Solar Air Heater With and Without Porous Medium, International Journal of Green Energy, (2011) 8:6, 643-654.

[34] Mohamed Salih, M.M., Alomar, O.R., Ali, F.A, Abd, H.M., An experimental investigation of a double pass solar air heater performance: A comparison between natural and forced air circulation processes, Solar Energy (2019) 193: 184-194.

[35] Hosseini, S.S., Ramiar, A., Ranjbar, A.A., Numerical investigation of natural convection solar air heater with different fins shape. Renewable Energy (2018) 117: 488-500.

[36] Singh, A.P., Kumar, A., Akshayveer, Singh, O.P., Natural convection solar air heater: Bell-mouth integrated converging channel for high flow applications, Building and Environment (2021) 187: 107367.

[37] Mesgar Pour, M., Heydari, A., Wongwises, S., (2021) Geometry optimization of double pass solar air heater with helical flow path, Solar Energy, 213, 67-80.

[38] Kalash, A.R., Shijer, S. S., Habeeb, L. J., (2020) Thermal Performance Improvement of Double Pass Solar Air Heater, Journal of Mechanical Engineering Research and Developments, 43:5 355-372.

[39] Singh, A.P., Akshayveer, Kumar, A., Singh, O.P., Designs for high flow natural convection solar air heaters, Solar Energy (2019) 193: 724-737.

[40] Pica, A.L., Rodono, G., Volpes, R., An experimental investigation of natural

convection of air in a vertical channel, Internationa Journal of Heat and Mass Transfer (1993) 36: 611-616.

[41] Duffie. J., Beckman, W., Worek, M., Solar Engineering Thermal Processes. Second edition (1994) 116.

[42] Cheng, X., Müller, U., Turbulent natural convection coupled with thermal radiation in large vertical channels with asymmetric heating, International Journal of Heat and Mass Transfer (1998) 41: 1681-1692.